Chemical Research in Toxicology

ARTICLE

pubs.acs.org/crt

Titanium Oxide Shell Coatings Decrease the Cytotoxicity of ZnO Nanoparticles

I-Lun Hsiao and Yuh-Jeen Huang*

Department of Biomedical Engineering and Environmental Sciences, National Tsing Hua University, 101, Section 2, Kuang-Fu Road, Hsinchu, Taiwan 30013

ABSTRACT: Although nanozinc oxide (nano-ZnO) is applied widely in photocatalysts and gas sensors and in biological fields, it can cause serious oxidative stress and DNA damage to mammalian cells. Our aim in this study was to reduce the cytotoxicity of nano-ZnO by coating it with a TiO_2 layer. We used a sol−gel method to synthesize core (nano-ZnO)/shell (TiO_2) nanoparticles (NPs) with various degrees of coating. Transmission electron microscopy and Raman spectroscopy confirmed that TiO_2 was coated on the nano-ZnO. Moreover, a decrease in the intensity of the pre-edge signal in Ti K-edge X-ray absorption near edge structure spectra revealed that the core/shell NPs had more Ti−O coordination than pure TiO_2 particles; in addition, the Zn K-edge extended X-ray absorption fine structure spectra revealed that after the ZnO NPs had been coated with TiO_2, the coordination number of the ZnO shell increased to 3.3 but that of the ZnZn shell decreased to 6.2, providing further evidence for the ZnO/TiO_2 core/shell structure. To ensure that the core/shell structures did indeed decrease the toxicity of nano-ZnO, we tested the effects of equal amounts of physical mixtures of ZnO and TiO_2 NPs for comparison, employing methyl tetrazolium (MTT), interleukin-8 (IL-8), lactate dehydrogenase (LDH), and 2′,7′-dichlorofluorescin diacetate (DCFH-DA) to assess the particle-induced cytotoxicity, inflammatory response, membrane damage, and intercellular reactive oxygen species (ROS). From X-ray diffraction patterns, we identified the TiO_2 shell as having an amorphous phase, which, unfortunately, exhibited slight cytotoxicity toward the human lung epithelial cell line (A549). Nevertheless, our core/shell nanostructures exhibited less oxidative stress toward A549 cells than did their corresponding ZnO/TiO_2 physical mixtures. In addition, a greater coating of TiO_2 decreased the toxicity of the ZnO NPs. It appears that the ZnO/TiO_2 core/shell structure moderated the toxicity of nano-ZnO by curtailing the release of zinc ions and decreasing the contact area of the ZnO cores.

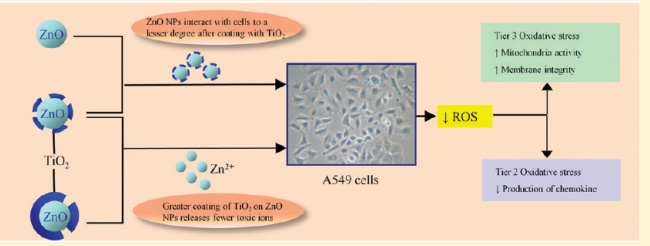

INTRODUCTION

In the past 20 years, the development of nanomaterials has focused primarily on single-component systems.[1−3] In recent years, however, the quest to improve the properties of nanomaterials (e.g., optical, electrical, and chemical) has led to methods for altering particle sizes, compositions, and surface characteristics.[4−6] Among such systems, heterostructured inorganic nanoparticles (NPs) have become popular because their quantum yields and photoluminescence tend to increase according to the quantum confinement effect,[7] making them applicable for use in solar cells and photocatalyst systems.[8,9] Furthermore, because of their small sizes, good stability in water, and stable fluorescence emissions, core/shell NPs have been applied as biosensors, contrast agents, and drug delivery assisting materials.[10−12] Therefore, many core/shell NPs have been developed, including SiO_2 on CdSe, Au on Fe_2O_3, and CdS on CdTe nanostructures.[13−15]

Nano-ZnO is regarded as a highly potentially applicable nanomaterial in the fields of photochemistry and biology.[16,17] When UV light is irradiated on nano-ZnO, however, photocorrosion can occur.[18] In addition, ZnO has low tolerance toward acidic solutions.[19] These phenomena are responsible for the decreased photocatalyst activity of nano-ZnO in aqueous solution. On the other hand, nano-ZnO exhibits high cytotoxicity and potentially damages cellular DNA, thereby limiting its applications in environmental and biological systems.[20−23] Therefore, several reports have appeared regarding the preparation of ZnO/TiO_2 core/shell NPs because TiO_2 has a higher dielectric constant, good tolerance toward acidic solutions, and good biocompatibility.[24−27] Such core/shell structures can also exhibit good optical properties and degradation efficiencies.[24,25]

Although core/shell NPs have unique properties, very few reports provide toxicity data. To date, studies of the toxicity of core/shell NPs have mostly centered on Cd-based QDs and magnetite NPs, in view of their wide applications in bioimaging.[28,29,31,32] Cadmium-containing QD NPs exhibit some cytotoxicity because of their release of cadmium ions (Cd^{2+}). As a result, many researchers are attempting to develop low-toxicity shell components to increase the biocompatibility of Cd-containing NPs. Cho et al. evaluated the cytotoxicity of CdTe and core/shell CdSe/ZnS NPs capped with mercaptopropionic acid, cysteamine, or *N*-acetylcysteine conjugated to cysteamine toward human breast cancer cells (MCF-7). Only the

Received: May 28, 2010
Published: February 22, 2011

dx.doi.org/10.1021/tx1001892 | *Chem. Res. Toxicol.* 2011, 24, 303–313

Table 1. Denomination of All Samples in This Study

sample	synthesis method	Ti/Zn molar ratio	synthesis temperature (°C)	coating time (h)	core species	morphology
ZnO-1	solvothermal	0	120			sphere-like
ZnO-2	solvothermal	0	180			sphere-like
TiO_2	sol−gel		25			amorphous
ZnO/TiO_2-1	sol−gel	0.31	25	24	ZnO-1	core/shell
ZnO/TiO_2-2	sol−gel	0.31	25	48	ZnO-1	core/shell
ZnO/TiO_2-3	sol−gel	0.31	25	24	ZnO-2	core/shell
ZnO/TiO_2-4	sol−gel	0.31	25	48	ZnO-2	core/shell
ZnO/TiO_2-5	sol−gel	0.63	25	24	ZnO-2	core/shell
ZnO/TiO_2-6	sol−gel	0.63	25	48	ZnO-2	core/shell
ZnO+TiO_2-1	ZnO-2 + TiO_2 (physical mixture)	0.31				sphere-like + amorphous
ZnO+TiO_2-2	ZnO-2 + TiO_2 (physical mixture)	0.63				sphere-like + amorphous

cysteamine-CdSe/ZnS core/shell QDs (10 μg mL^{-1}) exhibited no significant change in mitochondrial activity.[28] Furthermore, CdTe/CdS/ZnS core/shell/shell QDs have been tested for their effects on human erythroleukemia (K562) and human embryonic kidney (HEK293T) cell lines; MTT assays revealed no toxic effects, even at high concentrations (3 μM) and long exposure times (48 h).[29] The cytotoxicity of magnetite NPs appears to arise from radical production through Fenton- and Haber−Weiss-type reactions;[30] coating magnetite NPs with SiO_2, however, did not enhance their biocompatibility with osteoblasts.[31] Notably, coating a nontoxic shell onto a toxic core will decrease the real mass dosage of the original core NPs toward the cells; it will also increase the average size of the resulting NPs. If these two factors are not taken into consideration, researchers might overvalue the extent of the diminished toxicity of the particles.

In this study, we developed TiO_2-coated ZnO NPs that we expected would decrease the cytotoxicity of the original nano-ZnO toward human lung epithelial cells (A549). We compared the toxicity of the TiO_2-coated ZnO NPs with that of a physical mixture of TiO_2 and ZnO powders. Moreover, we fabricated the TiO_2-coated ZnO NPs with various degrees of coating, hypothesizing that the protective effect of the TiO_2 shell would increase with increased TiO_2 coating. We examined the physical characteristics of our core/shell NPs using transmission electron microscopy (TEM), X-ray diffraction (XRD), Raman spectroscopy, and X-ray absorption spectroscopy (XAS). We used inductively coupled plasma optical emission spectrometry (ICP-OES) to quantify the real Ti-to-Zn molar ratio and diffraction laser scattering (DLS) to measure the hydrodynamic sizes of the NPs in media. We evaluated the biological responses of our core/shell NPs through methyl tetrazolium (MTT), interleukin-8 (IL-8), lactate dehydrogenase (LDH), and intracellular ROS assays; finally, we evaluated the effect of the release of zinc ions from the ZnO and ZnO/TiO_2 NPs.

MATERIALS AND METHODS

Preparation of ZnO, TiO_2, and ZnO/TiO_2 NPs. A sol−gel method was used to synthesize the TiO_2-coated ZnO NPs.[24] Nano-ZnO cores of two different sizes were first derived using a solvothermal process, as developed by Du et al.[33] The ZnO NPs (160 mg) were added into a solution of ammonium hydroxide (28%, 18 mL; J. T. Baker, Phillipsburg) and absolute ethanol (Sigma−Aldrich, USA; 160 mL) and then sonicated for 1 h. Next, tetrabutylorthotitanate (TBOT, E. Merck, Germany; Ti/Zn molar ratio: 0.31 or 0.63) was added to deionized water (15 mL) and then sonicated for 10 min; this aqueous solution was gradually added dropwise (2 mL min^{-1}) into the organic solution, using a microtubing pump (MP-1000, EYELA, Tokyo), with vigorous stirring at room temperature. After 24 or 48 h, the precipitate was separated and collected through centrifugation and washed several times with absolute ethanol and water. Finally, the products were dried under vacuum at 50 °C for 24 h. Pure TiO_2 NPs were also prepared using the latter part of this procedure, with a reaction time of 24 h.

Denomination for the NPs. In Table 1, for core/shell NPs, the descriptor in front of the slash refers to the core ("ZnO") and that after it refers to the shell ("TiO_2"). Physical mixtures of NPs are described using the symbol "+". Samples having the same components are numbered.

Characterization of NPs. The morphologies and sizes of the NPs were characterized using TEM (TECNAI 20, Philips, Netherlands). For the core/shell NPs, the mean shell thickness was also determined from the TEM images. The thickest part of shell in each particle was measured; at least three particles were measured for each image. To prepare the samples, NPs were first dispersed in absolute ethanol (200 μg mL^{-1}) and sonicated (400 W, 40 kHz) for 30 min. Aliquots (4 μL) of the suspensions were deposited onto 200-mesh carbon-Formvar Cu grids. Finally, the solvents were evaporated in a vacuum oven for 1 h.

XRD analysis was performed to characterize the nanocrystalline structures of the ZnO/TiO_2 core/shell and pure TiO_2 NPs. An MXP18 X-ray diffractometer (MAC science, Japan) was scanned in the 2θ range from 25 to 75° with Cu-K$_{\alpha1}$ (λ = 1.54056 Å) radiation; the scan rate was 3° min^{-1}. To minimize deviation of the peak widths and to increase the precision of the pattern, a lower scan rate (1° min^{-1}) was used for the TiO_2 sample. The Debye−Scherrer equation was used to calculate the grain sizes of the ZnO cores.[34]

Raman and XAS spectra were recorded to further characterize the core/shell structures. Raman spectra were obtained using a Thermo-Fisher DXR Microscopy Raman system and a 532-nm laser line. XAS data were collected at the Ti K-edge (4966 eV) and Zn K-edge (9659 eV) with the BL-16A and BL-17C beamlines of the National Synchrotron Radiation Research Center (NSRRC) of Taiwan. Zinc element spectra were measured in transmission mode; Ti element spectra, in fluorescence mode. The nanopowders were covered with Kapton tape for pretreatment. The X-ray absorption near-edge structures (XANES) of the Ti K-edge were analyzed using WinXAS 3.1 software; the extended X-ray absorption fine structure (EXAFS) data were analyzed using IFEFFIT software. Fitting analysis in k_3-weighted Fourier transforms (3−12 Å) was applied to obtain a unique set of coordination number (CN), bond length, and σ^2 parameters.

The hydrodynamic diameters of the NPs in cell culture medium were measured using DLS with a Zetasizer nano ZS (Malvern Instruments, UK). Suspensions of NPs (at 200 μg mL^{-1}) were prepared in Dulbecco's modified Eagle's medium (DMEM High Glucose, with L-Glutamine, Biosera, UK). To decrease the agglomeration state, the dispersions were sonicated for 5 min in an ice bath using an ultrasonic probe (8 W, 22 kHz) (Ultrasonic Cell Disruptor, Misonix, USA).

The exact Ti and Zn compositions in the TiO_2-coated ZnO NPs were analyzed through ICP-OES (Jarrell-Ash, ICAP 9000, USA). Prior to ICP measurement, samples (25 mg) of the materials were completely dissolved in an acid solution [HNO_3 (2 mL), HCl (2 mL)] in a Teflon-coated autoclave, with digestion at 443 K for 6 h.

A549 Cell Line. The human lung carcinoma epithelial cell line (A549; BCRC-60074) was purchased from Bioresource Collection and Research Center, Taiwan. Cells were cultured in DMEM supplemented with 10% fetal bovine serum (FBS) and 1% penicillin, streptomycin, and amphotericin mixture; they were then cultivated in T25 flasks at 37 °C in a humidified atmosphere of 5% CO_2/95% air.

Preparation of Stock Solution and Sample Exposure. Nanopowders suspended (20,000 μg mL^{-1}) in dimethyl sulfoxide (DMSO; Sterile, Sigma−Aldrich) were used as stock solutions. Prior to dilution, probe sonication (5 W, 90 s) was performed to decrease the degree of aggregation. Particle concentrations within the range from 50 to 1.56 μg mL^{-1} were selected to estimate the NPs' cytotoxicity; all samples for cytotoxicity testing were dispersed in serum-free DMEM. The DMSO concentration never exceeded 0.25% in any of the treatment groups. The control medium also incorporated 0.25% DMSO. All media were sonicated (400 W, 40 kHz) in an ultrasonic cleaner (DC-400H, Delta, Taiwan) for 10 min to break up the agglomerates. The A549 cells were exposed to samples after 24 h of cell attachment. The cell densities in the cytotoxicity assays were as follows: 4×10^4 cells mL^{-1} in 96-well plates for MTT and IL-8 assays; 1×10^5 cells mL^{-1} in 96-well plates for LDH assay; and 2×10^5 cells mL^{-1} in six-well plates for the intracellular ROS analysis. A lower cell density was used in the MTT assay because the absorption of MTT formazan, which was measured by the ELISA reader, would be too high to evaluate the cell viability (optical density >2) when the cell density was at or above 1×10^5 cells mL^{-1}. Because the samples used for the IL-8 assay were obtained from exposed suspensions, the cell density was the same as that in the MTT assay. Although ROS analysis through flow cytometry required at least 10,000 living cells, some cells would die during the exposure processes and be removed during the washing steps; therefore, we required more cells to complete the experiment.

Cytotoxicity Assays. *MTT Metabolism Assay.* The cells were exposed to 1.56, 3.13, 6.25, 12.5, 25, and 50 μg mL^{-1} solutions of the NPs for 24 or 48 h. After exposure, the cell medium was aspired and the aliquots transferred to a clean flat-bottom plate for subsequent IL-8 or LDH analysis. Cells were washed once with 1× phosphate-buffered saline (PBS) to remove NPs that might have caused misleading readouts because of Zn^{2+}-MTT dye interference and particle absorption effects at high dosage.[35] MTT 3-(4,5-dimethylthiazol-2-yl)-2,5-diphenyltetrazolium bromide (Aldrich)/DMEM (with 10% FBS) solution (0.5 mg mL^{-1}, 200 μL) was added to each well; the plate was then incubated for 3 h. After incubation, the MTT solution was discarded, and DMSO (200 μL) was added. Finally, the absorbance was measured at 570 nm using a tunable microplate reader (VersaMax, Molecular Devices, USA). The MTT activity (%) was calculated using the expression [cell number of testing samples]/[cell number of control] × 100. Cell numbers were derived from a standard curve (at log parameter), which was obtained after seeding serially diluted cells (from 1×10^5 to 1.56×10^3 cells mL^{-1}) in a 96-well plate.

IL-8 Assay. The production of pro-inflammatory factor IL-8 was analyzed using a Human IL-8 ELISA kit (PeproTech, USA). First, capture antibody (0.5 μg mL^{-1}, 100 μL) was added to each well in a 96-well ELISA plate (Maxisorp, Nunc, USA) and incubated overnight at room temperature. Next, blocking solution (200 μL) was added to each well, followed by incubation for 1 h. Third, the sample (100 μL) and IL-8 standard (16−2000 pg mL^{-1}) were added to each well, followed by incubation for 2 h. Fourth, the detection antibody (0.25 μg mL^{-1}, 100 μL) was added, followed by incubation for 2 h. Fifth, diluted adivin/HRP conjugate (1:2000 solution, 100 μL) was added to each well, followed by incubation for 30 min. Between each of these steps, the solution in each well was aspirated and washed four times with washing buffer. Next, the color reaction mixture (TMB, 100 μL) was added into each well. After sufficient color development (20 min at room temperature), the stop solution (2 M H_2SO_4, 50 μL) was added to each well. Finally, the absorbance was measured at 450 nm using a tunable microplate reader.

LDH Assay. Lactate dehydrogenase (LDH) activity was measured using a lactic dehydrogenase−based in vitro toxicology assay kit (TOX7, Sigma−Aldrich). This assay is based on the reduction of NAD^+ by LDH; the rate of NAD^+ reduction is equal to the stoichiometric conversion of a tetrazolium dye, detected at 490 nm. For comparison of the cytotoxicities of the core/shell NPs and the ZnO+TiO_2 mixture of NPs, cells were exposed to 5, 10, and 25 μg mL^{-1} solutions of the particles for 48 h. For evaluation of the cytotoxicities of NPs having various shell thicknesses, cells were exposed to 5, 10, 25, and 50 μg mL^{-1} concentrations of the NPs for 48 h. After exposure, the cell medium was transferred to a microtube and centrifuged at 250*g* for 4 min. The supernatant (70 μL) was transferred to a clean flat-bottom plate and subjected to enzymatic analysis. The LDH activity was determined using the expression [sample absorbance]/[control absorbance] × 100.

Analysis of Intracellular ROS. The production of intracellular ROS was measured using 2′,7′-dichlorofluorescin diacetate (DCFH-DA, Sigma−Aldrich) as a reactive fluorescent probe. When DCFH-DA is absorbed by cells, esterase transforms it into nonfluorescent HDCF, which is then oxidized to fluorescent dichlorofluorescin (DCF) by intracellular ROS; the fluorescence is then detected at 528 nm after excitation at 488 nm. After exposure of the cells to NP solutions at 5 and 25 μg mL^{-1}, DMEM was removed, and then the cells were rinsed with 1× PBS. Next, 1× trypsin-EDTA (1 mL) was added to remove adherent cells from the surface of the flask. The DCFH-DA working solution, which was obtained after diluting 40 mM DCFH-DA stock solution (in ethanol) to 40 μM in DMEM without serum, was added to each well, followed by incubation for 30 min. The solutions were then centrifuged (1000*g*, 3 min) and the supernatant medium removed entirely. Prior to measurement, the cells were resuspended in 1× PBS. The fluorescence was determined using a BD FACSCanto flow cytometer (BD Science, San Jose, CA), with 10,000 cells collected. The mean fluorescence intensity was analyzed using FCS Express data analysis software (v. 3.0).

Analysis of Zinc Ions in DMEM. To examine the dissolution of ZnO NPs in DMEM, the concentrations of zinc ions released from ZnO and ZnO/TiO_2 NPs were measured. First, samples of stock solution were diluted (1:400) in serum-free DMEM and left for 24 h at room temperature. Next, aliquots (1 mL) were centrifuged (14,000*g*, 20 min) and diluted (1:40, v/v) with deionized water. Prior to analysis, nitric acid was added to a final concentration of 1%. Finally, the resulting zinc concentration was measured using ICP-MS (SCIEX ELAN 5000 ICP-MS, Perkin−Elmer, USA). The zinc concentration was determined from the intensity of the signal of the Zn isotope having a mass-to-charge ratio (m/z) of 66; an external calibration method was used.

Statistics. Toxicity effects of the various NPs on the cell cultures were analyzed statistically, with a $p < 0.05$ significance level, using a two-tailed Student's *t*-test. All data are expressed as the means ± SDs.

RESULTS

Particle Characterization (TEM, XRD, Zetasizer, ICP-OES). TEM images revealed that the two ZnO NPs had different size distributions (32−95 nm for ZnO-1 and 50−122 nm for ZnO-2), but the same sphere-like morphology. We used these loosely aggregated particles as core moieties of the nanocomposites (Figure 1 and Table 2). The TiO_2 NPs formed a compact aggregate; their particle size was generally larger (90−160 nm) than that of the ZnO NPs, and their shape was nonuniform. After

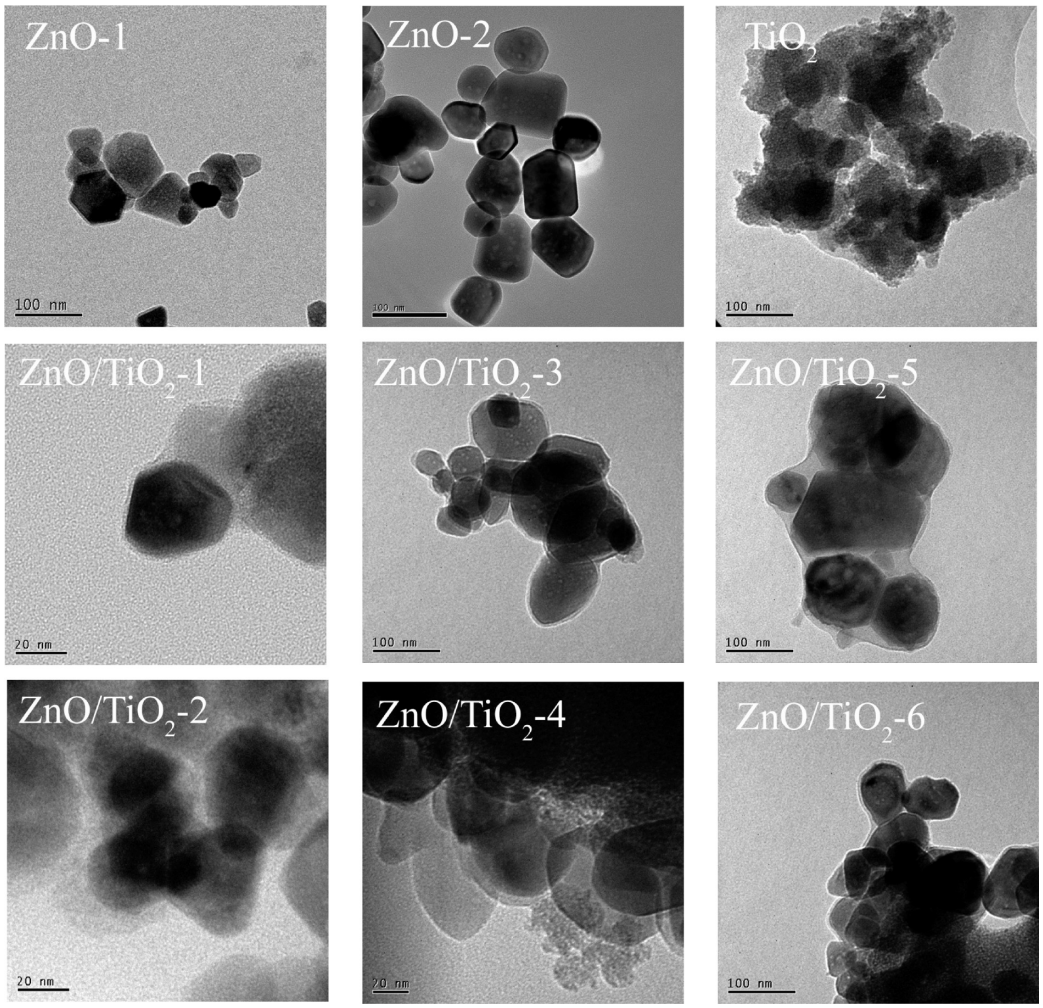

Figure 1. TEM images of the ZnO and TiO_2 NPs and their core/shell structures.

Table 2. Particle Characteristics

particle[a]	size distribution (nm)	ZnO diameter[b] (nm)	mean shell thickness (nm)	hydrodynamic size in DMEM[c] (nm)	PdI width[d]	molar ratio[e]
ZnO-1	32−95	25		765 ± 35	0.30	
ZnO-2	50−122	38		975 ± 58	0.12	
TiO_2	90−160			1081 ± 73	0.27	
ZnO/TiO_2-1	43−83	27	2.5	1246 ± 189	0.19	0.25
ZnO/TiO_2-2	43−66	24	8.3	1280 ± 204	0.23	0.32
ZnO/TiO_2-3	45−154	37	3.8	1221 ± 85	0.36	0.35
ZnO/TiO_2-4	57−90	38	5.7	1177 ± 95	0.31	0.37
ZnO/TiO_2-5	68−200	36	5.3	1044 ± 81	0.30	0.65
ZnO/TiO_2-6	54−130	38	5.5	1139 ± 163	0.40	0.64

[a] Denomination of particles defined in Table 1. [b] Grain size of ZnO core, estimated from XRD data and calculated using the Debye−Scherrer equation. [c] All DLS measurements were performed in triplicate. [d] Polydispersity index (PdI), a size distribution parameter derived from the coefficient of the correlation function. [e] Practical molar ratio of TiO_2 and ZnO in core/shell NPs was measured using ICP-OES.

coating with TiO_2, we detected a thin layer on the surface of the nano-ZnO and found that increasing the Ti-to-Zn molar ratio from 0.31 to 0.63 provided a slightly thicker shell (Figure 1); moreover, the shell became thicker upon extending the reaction time from 24 to 48 h. Table 2 lists the average layer thicknesses for all particles. Although TiO_2 was coated on the ZnO using either set of conditions, a small part of ZnO remained uncovered.

In the XRD spectra of the two nano-ZnO samples (Figure 2b and e), all of the characteristic peaks matched well with those of hexagonal crystalline ZnO (JCPDS no. 36-1451). The grain sizes of ZnO were 25 and 38 nm, calculated using the Debye−Scherrer equation. XRD analysis of the TiO_2 NPs (Figure 2a) did not reveal any diffraction peaks for a crystalline structure (anatase or rutile). Because the range of sizes of the TiO_2 NPs was ca. 90−160 nm (i.e., they were not particularly small), we

dx.doi.org/10.1021/tx1001892 |*Chem. Res. Toxicol.* 2011, 24, 303–313

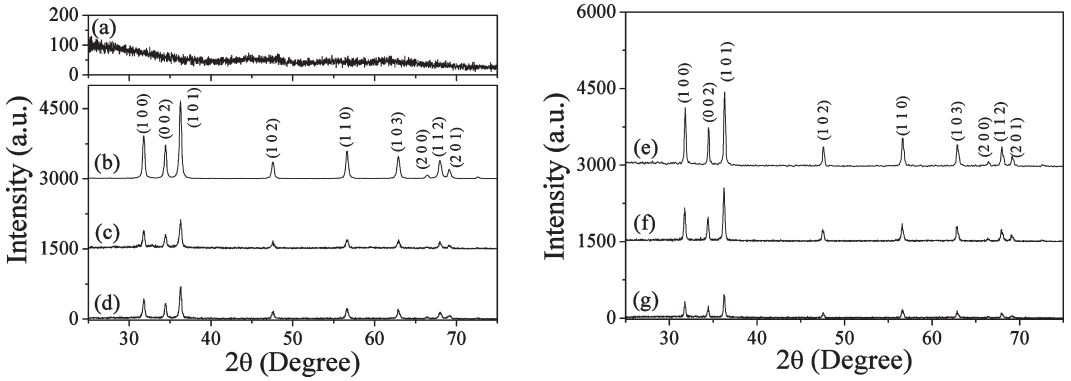

Figure 2. Typical XRD patterns of the synthesized nanostructures. (a) TiO_2; (b) ZnO-1; (c) ZnO/TiO_2-1; (d) ZnO/TiO_2-2; (e) ZnO-2; (f) ZnO/TiO_2-3; (g) ZnO/TiO_2-5.

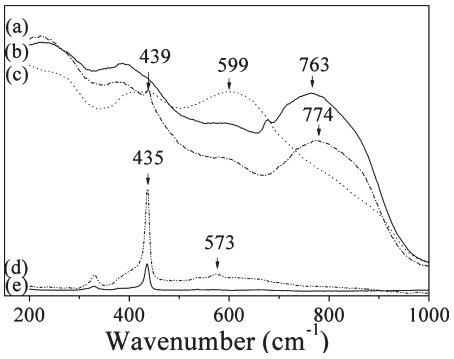

Figure 3. Raman spectra of the synthesized nanostructures. (a) ZnO/TiO_2-1, (b) ZnO/TiO_2-5, (c) TiO_2, (d) ZnO+TiO_2-2, and (e) ZnO-2.

speculated that the phase of TiO_2 was amorphous. After coating the ZnO NPs with TiO_2, the shapes and positions of the signals in the XRD patterns remained relatively unchanged when compared with those of the pure hexagonal ZnO NPs; again, we observed no characteristic peaks for crystalline TiO_2 (Figure 2c, d, f, and g). Notably, however, the baselines of the XRD spectra of the ZnO/TiO_2 core/shell structures were rougher than those of the pure ZnO NPs. Because the procedures for preparing TiO_2 and core/shell NPs were identical, with the exception of the addition of ZnO, these findings suggest that the TiO_2 shells were also amorphous.

We used a DLS method to measure the hydrodynamic sizes of the core/shell NPs in serum-free media.[36] The particle diameters of all the coated samples increased from those of the primary NPs. In addition, the hydrodynamic sizes of the ZnO/TiO_2 NPs (ca. 1100 nm) were all larger than those of the ZnO cores; the TiO_2 layers coated on the ZnO-2 NPs had slightly smaller hydrodynamic sizes than those on the ZnO-1 NPs. ICP-OES measurements provided us with the real Ti/Zn molar ratios for the as-prepared core/shell NPs; the molar ratios of the ZnO/TiO_2 were similar to their stoichiometric ratios (Table 2).

Confirming the Core/Shell Structure (Raman, XAS). Figure 3 displays Raman spectra of the ZnO, TiO_2, TiO_2-coated ZnO, and physical mixtures of TiO_2 and ZnO NPs. For the ZnO-2 NPs, we observe a vibration peak at 435.2 cm^{-1} [E_2 vibration mode[37]]. For the TiO_2 NPs, broader peaks appear at 439 and 599 cm^{-1} [E_g and $A_{1\ g}$ vibration modes[38]]. After coating with TiO_2, we observe large blue shifts of the signal from typically 599 cm^{-1} for TiO_2 to 774 cm^{-1} and 763 cm^{-1} for ZnO/TiO_2-1 and ZnO/TiO_2-5, respectively. However, if the ZnO and TiO_2 NPs were just mixtures, the large blue shift of the signal for TiO_2 could not be observed.

Table 3. Structural Parameters around Zn Atoms in ZnO and ZnO/TiO_2 Nanocomposites

	ZnO shell			ZnZn shell		
particle	CN[a]	R[b]	$\sigma^2/10^{-4}$ Å^2	CN	R	$\sigma^2/10^{-4}$ Å^2
bulk	3.4	1.93	36	11.4	3.21	92
ZnO-1	2.6	1.96	37	7.6	3.21	87
ZnO-2	3.0	1.96	34	9.5	3.21	87
ZnO/TiO_2-1	3.3	1.95	46	6.2	3.24	79
ZnO/TiO_2-5	3.3	1.95	42	6.9	3.23	82

[a] Coordination number. [b] Bond distance.

Figure 4A presents an overlay of the Zn K-edge EXAFS spectra $k^3\chi(k)$ for bulk ZnO and the synthesized NPs. The broad peaks at ca. 1.9 Å represent the Zn atoms in the ZnO shell; the neighboring peaks at ca. 3.2 Å represent those in the ZnZn shell. The area of each peak represents the coordinated state of the Zn atoms. We used IFEFFIT software to determine the bond lengths (R) and CNs, assuming errors in the values of CN to be ±10% (±0.02 Å) for R and ±20% for the Debye−Waller factors (σ^2). Figure 4B and Table 3 present the parameters resulting from curve fitting. The ZnO-1 and ZnO-2 NPs had lower values of CN for their ZnO (2.6 and 3.0, respectively) and ZnZn (7.6 and 9.5, respectively) shells, relative to those of the bulk ZnO. After coating these two NPs with TiO_2, the values of CN of the ZnO shells both increased to 3.3, but those of the ZnZn shells decreased further, to 6.2 and 6.9 for ZnO/TiO_2-1 and ZnO/TiO_2-5, respectively. In addition, the bond lengths of the ZnZn shells were slightly longer than those of the pure nano-ZnO samples.

Figure 5 displays experimental Ti K-edge XANES spectra of the pure TiO_2 shell and a series of ZnO/TiO_2 core/shell NPs. In all of these spectra, the pre-edge region reveals only one obvious signal, confirming the amorphous structure.[39] The intensity and position of these specific peaks in the pre-edge region is highly correlated to the symmetry environment of the Ti atoms.[40] The inset to Figure 5 presents a plot of the height and position of each pre-edge peak; although the peak energy in all samples appeared at the same position (4.9712 eV), as the TiO_2 formed a shell, the normalized peak height decreased from 0.32 to ca. 0.25. Combining this information with the results obtained by Farges

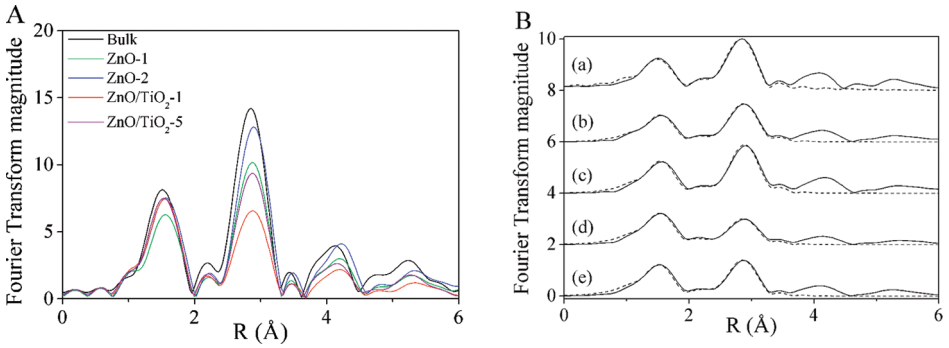

Figure 4. (A) k_3-Weighted EXAFS spectra for the ZnO and ZnO/TiO_2 NPs. (B) Curve-fitting results: (a) bulk ZnO, (b) ZnO-1, (c) ZnO-2, (d) ZnO/TiO_2-1, and (e) ZnO/TiO_2-5. IFEFFIT fitting results are provided as dashed lines.

et al.,[40] we conclude that the amorphous TiO_2 NPs featured between six- and five-coordinate Ti atoms (TiO), consistent with the model result (CN = 5.3) reported by Zhang et al.[39] In contrast, the core/shell structures appeared to favor a six-coordinate Ti environment.

Cytotoxicity of ZnO Cores and TiO_2 Shells. Before evaluating the cytotoxicities of the core/shell NPs, we used separate MTT assays to compare cell proliferations in response to various concentrations of TiO_2 and ZnO cores (Figure 6). Although ZnO-2 and the amorphous TiO_2 NPs had similar primary and secondary sizes, they exhibited significantly different cytotoxicities toward A549 cells. Whereas the cell viability decreased dramatically when we exposed the A549 cells to ZnO-2 for 24 h (to 8.6% at 50 μg mL^{-1}), the situation for TiO_2 was moderate (to 70% at 50 μg mL^{-1}). Because amorphous TiO_2 is somewhat toxic, we would expect the core/shell NPs to also cause cell death to a certain extent. Therefore, if we are to demonstrate that the TiO_2-coated ZnO NPs exhibited decreased toxicity relative to that of ZnO, we could not ignore the toxicity of TiO_2 itself.

Cytotoxicities of TiO_2-Coated ZnO NPs and Physical Mixtures of TiO_2 and ZnO NPs. To assess the cytotoxicities of the synthesized core/shell NPs, we used assays based on cell proliferation (MTT), the production of pro-inflammatory factor (IL-8), LDH activity (LDH), and the release of intracellular ROS (DCFH-DA). For comparison, we also determined the cytotoxicities of physical mixtures of ZnO-2 and TiO_2 NPs at the same compositions as those of the core/shell NPs. Using this method, we avoided the possibility of ignoring the real mass dosage of the ZnO core. Furthermore, the agglomeration size of the mixed NPs was similar to that of the core/shell NPs (1157 ± 55 nm), almost ruling out the effect of size on cytotoxicity. At NP concentrations of 50, 25, 12.5, and 6.25 μg mL^{-1}, the viabilities of A549 cells after exposure for 24 h to ZnO/TiO_2-3 were 47, 63, 64, and 75%, respectively; to ZnO/TiO_2-5, they were 18, 66, 88, and 97%, respectively (Figure 7A). These two core/shell NPs exhibited intermediate toxicity between those of the ZnO-2 and TiO_2 NPs. Relative to their corresponding physical mixtures, both of the core/shell NPs exhibited lower toxicities (i.e., higher cell viabilities). In the IL-8 production assay (Figure 7B), the ZnO/TiO_2-5 NPs induced less chemokine production than did the ZnO/TiO_2-3 NPs from each cell (0.0002/0.001 vs 0.0016/0.0043 pg $cell^{-1}$ at 12.5/25 μg mL^{-1}, respectively). The corresponding physical mixtures induced more chemokine production than did their core/shell forms (0.0017 and 0.0039 pg $cell^{-1}$ for the ZnO+TiO_2-2; 0.0056 and 0.0062 pg $cell^{-1}$ for the ZnO+TiO_2-1).

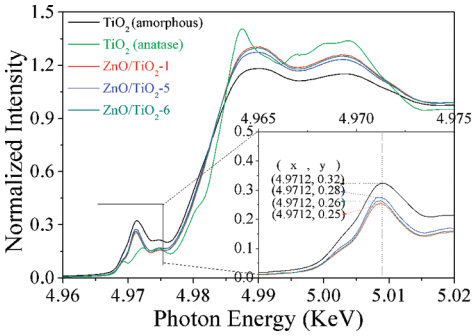

Figure 5. Ti K-edge XANES spectra of amorphous and anatase TiO_2 and ZnO/TiO_2 core/shell nanocomposites. Inset: expanded view of the pre-edge section; heights and energies of the pre-edge signals are provided.

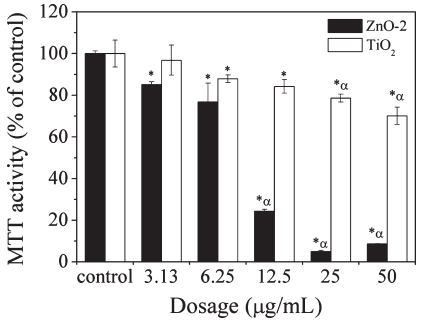

Figure 6. Cytotoxicity patterns of ZnO-2 and TiO_2 NPs after 24-h exposure to A549 cells. Significance effects: * $p < 0.05$ vs control cells; $^{\alpha}p < 0.05$ vs cells exposed to 3.13 μg mL^{-1}.

Increased LDH release relative to that of the control (Figure 7C) was evident at a significant level only at 25 μg mL^{-1} exposure. The ZnO+TiO_2-1 sample induced a greater LDH release than did its core/shell form (nearly double that of the control). In comparison with the control group, the DCF fluorescence intensities (Figure 7D) increased to 113 and 173% at ZnO/TiO_2-3 concentrations of 5 and 25 μg mL^{-1}, respectively; for the ZnO+TiO_2-1 sample, the A549 cells provided even greater increases in intracellular ROS production (181 and 246%, respectively).

Cytotoxicities of NPs with Different Degrees of Coating. Because the cytotoxicities of the core/shell NPs were higher than

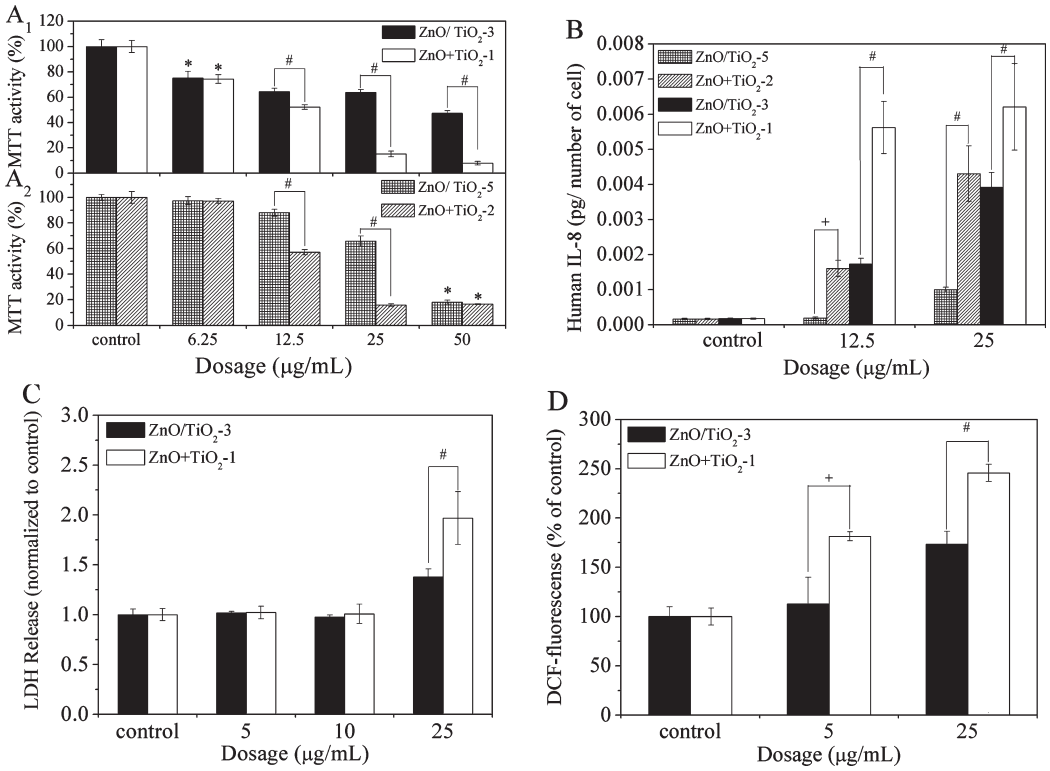

Figure 7. Metabolism activity, production of pro-inflammatory factor, LDH activity, and intracellular H_2O_2 levels of A549 cells after exposure to various concentrations of ZnO/TiO_2 core/shell nanocomposites and corresponding amounts of physically mixed ZnO and amorphous TiO_2 NPs. (A) MTT assay (incubation time, 24 h); (B) IL-8 assay (incubation time, 24 h); (C) LDH assay (incubation time, 48 h); (D) DCF fluorescence (incubation time, 24 h). *Statistically different from the control, $p < 0.05$; $^{+}$Statistically different between the treated groups, but one is not significantly different from the control. $^{\#}$Statistically different both from the control and between the treated groups.

that of amorphous TiO_2, we were interested in determining whether the cytotoxicity would decrease upon increasing the coating level. We compared the effects of two series of core/shell NPs having different shell thicknesses. Figure 8A reveals no significant differences in MTT activity after 24 h between the thinner (ZnO/TiO_2-1 and ZnO/TiO_2-3)- and thicker-shell (ZnO/TiO_2-2 and ZnO/TiO_2-4) NPs at low concentration (<25 μg mL^{-1}). At 50 μg mL^{-1}, however, the thicker-shell NPs (52 and 66%, respectively) led to higher cell viability than did the thinner-shell NPs (42 and 47%, respectively). Analysis of the amounts of human IL-8 after 48 h revealed that, below 12.5 μg mL^{-1} exposure, none of the samples had significant inflammatory effects on A549 cells (Figure 8B). In addition, the ZnO/TiO_2-4 NPs, which had a thicker shell, induced less pro-inflammatory factor than did the ZnO/TiO_2-3 NPs at 12.5 (62 vs 79 pg mL^{-1}) and 25 μg mL^{-1} (140 vs 180 pg mL^{-1}), whereas the ZnO-1-based core/shell NPs did not exhibit any such differences.

Higher LDH activities appeared (Figure 8C) only when the exposure concentration was greater than 12.5 μg mL^{-1}; a significant difference in the level of LDH released from the A549 cells appeared only for the ZnO/TiO_2-3 and ZnO/TiO_2-4 NPs (2.3- and 1.9-fold increases, respectively). The ZnO-2-based core/shell NPs also caused increases in DCF fluorescence intensity (Figure 8D) from the A549 cells at 25 μg mL^{-1}, but only the ZnO/TiO_2-3 NPs induced more ROS than did the control group (173% of control).

Figure 9 reveals the effect of the TiO_2 coating on the dissolution rate of ZnO nanoparticles in cell culture medium (DMEM). The uncoated ZnO released more zinc ion than did the TiO_2-coated ZnO at all lengths of time (3, 6, 24, and 48 h) and at all concentrations (10 and 50 ppm). Moreover, as more TiO_2 was coated onto ZnO, lower zinc ion concentrations were observed.

DISCUSSION

We produced ZnO/TiO_2 core/shell NPs using a sol−gel method, and employed several methods to demonstrate their core/shell structures. TEM images revealed darker cores and lighter shells for the NPs obtained under various conditions (Ti/Zn ratios, coating times), presumably because the atomic number of Zn (65) is higher than that of Ti (47). By comparing its physical mixtures, Raman spectra of the TiO_2-coated ZnO NPs revealed a large blue-shift of the signal of the $A_{1\ g}$ mode, most likely related to transformation of the particle structure to the shell form,[41] altering the molecular polarizability.

EXAFS data revealed that the nano-ZnO had lower values of CN for its ZnO and ZnZn shells than did the bulk material, presumably because the technique is more sensitive to surface atoms. On the surfaces of the nano-ZnO particles, the Zn atoms "bond" to fewer O atoms, and so do the other Zn atoms.[42] Using the same idea, if a ZnO NP is coated with a layer of TiO_2, the Zn atoms will "bond" to more O atoms (increased CN) at the surface of the core (from TiO_2). The reason for the decreasing value of CN of the ZnZn bonds and their enlarged bond length might suggest that some Ti atoms had become incorporated at Zn sites in the ZnO lattice. Further evidence for the core/shell

dx.doi.org/10.1021/tx1001892 |Chem. Res. Toxicol. 2011, 24, 303–313

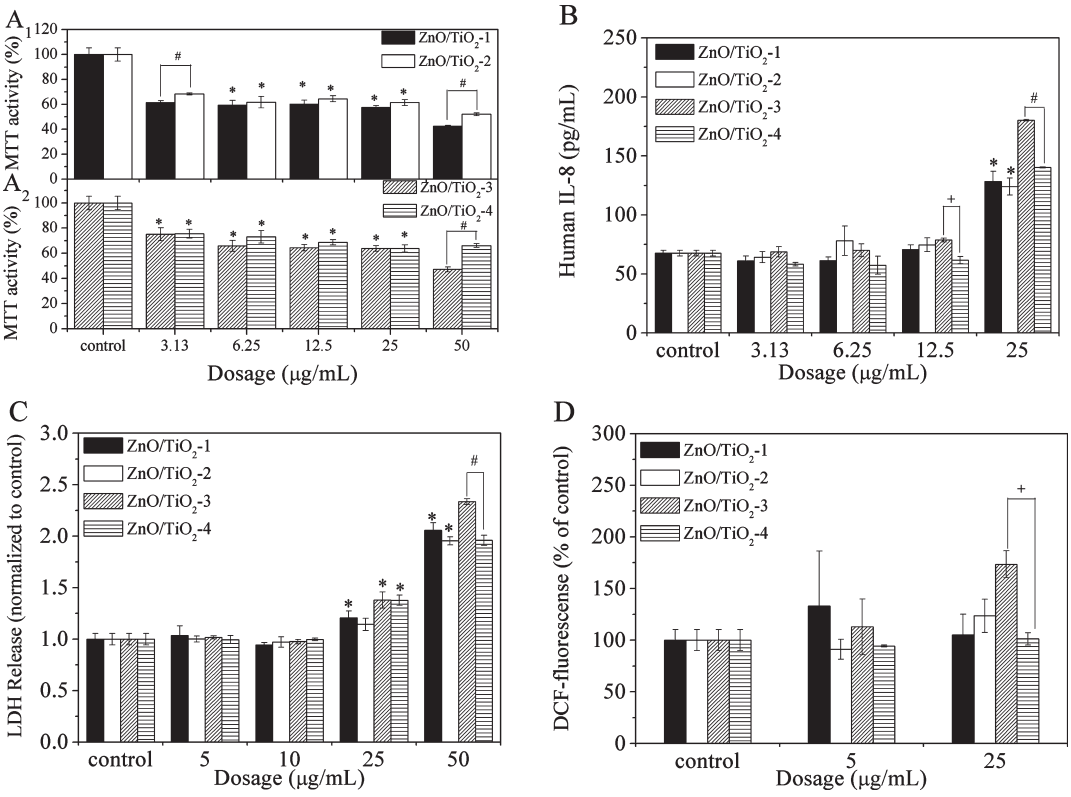

Figure 8. Metabolism activity, production of pro-inflammatory factor, LDH activity, and intracellular H_2O_2 levels of A549 cells after exposure to ZnO/TiO_2 core/shell nanocomposites having various shell thicknesses and core diameters. (A) MTT assay (incubation time, 24 h); (B) IL-8 assay (incubation time, 48 h); (C) LDH assay (incubation time, 48 h); (D) DCF fluorescence (incubation time, 24 h). *Statistically different from the control, $p < 0.05$; $^{+}$Statistically different between the treated groups, but one is not significantly different from the control. $^{\#}$Statistically different both from the control and between the treated groups.

structures was provided by the pre-edge signals in the Ti K-edge XANES spectra. We attribute this specific pre-edge signal to transitions from the Ti 1s energy levels to bind Ti 3d (or O 2p) molecular orbitals.[40] When there are more O atoms near Ti atoms, destructive interference can lead to a decreased intensity of this specific peak, just beyond the Fermi energy. Spectra of the core/shell NPs, which feature a more-distorted coordination environment, confirmed that the interactions between the TiO_2 shell and the ZnO core were sufficiently strong to modify the electronic states of the Ti atoms for the 1s−3d transition.[43]

In this study, we expected the TiO_2 coatings to decrease the toxicity of the nano-ZnO particles, which are potentially toxic to the environment and our bodies. In terms of antibacterial activity, 67-nm ZnO NPs have resulted in a 48% reduction in growth of Gram-negative *E. Coli* at 1000 ppm, with 98% growth reduction of Gram-positive *B. subtilis* occurring at only 50 ppm.[20] In terms of cytotoxicity toward mammalian cells, 50−70-nm (mean size) nano-ZnO particles have led to dramatically damaged mitochondrial function of mouse neuroblastoma (Neuro-2A), from 50 to 100 ppm.[44] A steep drop in A549 cell viability has also been found at 8−25-ppm dosages of 70-nm nano-ZnO.[44] In contrast, 66-nm TiO_2 has provided a 44% growth reduction in *E. Coli*, but no growth reduction in *B. subtilis*, at 50 ppm.[20] Furthermore, TiO_2 NPs (<40 nm) have no measurable effect on Neuro-2A cells at concentrations of less than 200 ppm.[44] In addition, significant differences in A549 cytotoxicity, relative to that of the control, have been noted only when the dosage of TiO_2 NPs was greater than or equal to 50 ppm.[45] Our cytotoxicity data for nano-ZnO and nano-TiO_2 were consistent with these findings, but we also found that cell death still occurred when the cells were exposed to TiO_2 at concentrations greater than 6.25 μg mL^{-1}. XRD and Ti K-edge XANES spectra revealed that the TiO_2 NPs and the TiO_2 shells of the ZnO/TiO_2 core/shell NPs were all amorphous. The anatase, rutile, and amorphous structures of TiO_2 are known to display different cytotoxicities.[46,47] For example, 50-nm amorphous TiO_2 NPs reveal a significantly different toxicity in comparison with those of its anatase and rutile forms at low concentrations (5−50 μg mL^{-1}) in mouse keratinocyte cells; other research has suggested that the ability of the different forms of TiO_2 NPs to generate ROS follows the order amorphous > anatase > rutile.[47] Nevertheless, we found that the ZnO NPs coated with TiO_2 layers exhibited cell viabilities different from those of amorphous TiO_2 NPs. In addition, the TiO_2-coated ZnO NPs were less toxic than were equal amounts of physically mixed TiO_2 and ZnO NPs. These two results indicate that the TiO_2 shells provided A549 cells with effective protection against cytotoxic ZnO NPs.

We detected the amount of IL-8 chemokine, an important mediator of pulmonary inflammation, to evaluate an intermediate level (Tier 2) of oxidative stress to human lung epithelial cells.[48] Nano-ZnO has been reported to elicit a pronounced IL-8 mRNA level response at a dosage of 10 μg mL^{-1} to human aortic endothelial cells (HAECs) and at a dosage of 0.3−8.5 μg cm^{-2} to A549 cells.[23,49] Ultrafine TiO_2 particles can also trigger inflammatory responses to A549 cells; these responses appear to be driven by the specific surface area of the particles, even if they

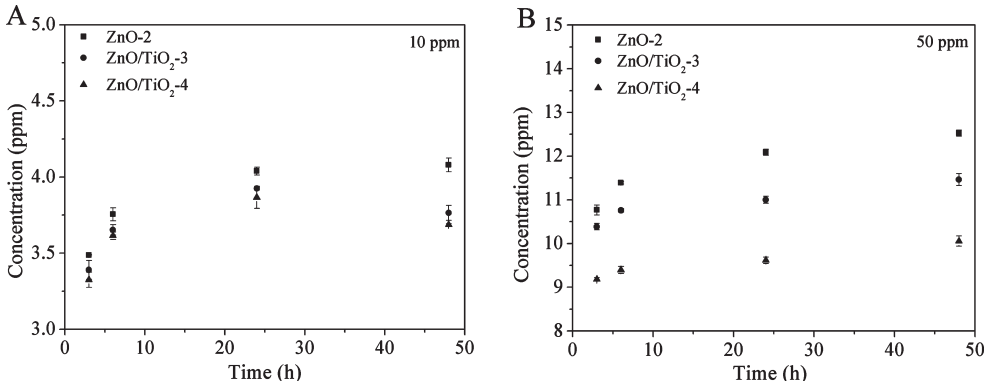

Figure 9. ICP-MS analyses of zinc ions released from ZnO-2, ZnO/TiO_2-3, and ZnO/TiO_2-4 core/shell nanocomposites after 3, 6, 24, and 48 h in DMEM. Particle suspension: (A) 10 ppm; (B) 50 ppm.

have formed large aggregates.[50] In this present study, we found that ZnO+TiO_2 NP mixtures induced more IL-8 than did their corresponding core/shell NPs, presumably because the mixed NPs had more opportunity to undergo ZnO particle−cell interactions. One study has demonstrated that ZnO particles require cell contact to impart toxicity,[51] consistent with our contention.

The cytotoxicities of TiO_2 and ZnO NPs are presumably associated mainly with membrane damage. Indeed, the physically mixed NPs also provided higher LDH activity at 25 μg mL^{-1} than did the core/shell NPs. ROS species (including superoxides, hydrogen peroxide, hydroxyl, and other oxygen radicals) can cause lipid peroxidation and protein and DNA damage within cells. In this present study, we used the fluoroprobe DCFH-DA to measure the level of intracellular ROS. There is much evidence suggesting that ZnO and TiO_2 NPs induce ROS production, leading to cell death, in various types of mammalian cells.[47,50,52−54] Nevertheless, the exact mechanism of ROS formation remains unknown. Our results revealed that more ROS generation occurred upon exposure to the ZnO+TiO_2 NP mixtures, indicating that the core/shell structures induced less oxidative stress to the A549 cells.

From a study of the ZnO-1-based and ZnO-2-based core/shell NPs, we found that thicker-shell species were less cytotoxic; unfortunately, this behavior occurred only at high concentrations (>25 μg mL^{-1}). The inflammatory response, LDH activity, and ROS generation data allowed us to reach the same conclusion. Increasing the coating time of the nano-ZnO increased the proportion of the coating and provided a thicker shell. The former contributed to a reduction in the oxidative stress level (relative to that of nano-ZnO), whereas both were responsible for the decrease in the rate of zinc ion release. The formation of dissolved zinc ions from nano-ZnO particles has a critical role affecting their toxicity.[21,30,55] One study even demonstrated that if the dissolution rate of ZnO NPs decreased through iron doping, the zinc ion-mediated cytotoxicity pathway which included ROS generation, intracellular calcium flux, mitochondria perturbation, and plasma membrane leakage would be diminished.[56] ICP-MS analysis revealed that the thinner-shell NPs released more Zn^{2+} ions than did the thicker-shell NPs after 24-h incubation in DMEM (Figure 9). This finding is consistent with our toxicity data. We also found that the ZnO-2 series of core/shell NPs had more potential for inducing oxidative stress than did the ZnO-1 series, presumably because the aggregation size of the former was slightly smaller than that of the latter and, therefore, more particles could be internalized within cells. Although TiO_2 coatings can decrease the cytotoxicity of nano-ZnO, the issue of biocompatibility remains to be improved.

In conclusion, we have fabricated TiO_2-coated ZnO core/shell NPs and obtained convincing evidence for their core/shell structures. By comparing the cytotoxicities of ZnO and TiO_2 (amorphous) NPs, we found that our TiO_2 NPs were less toxic than our ZnO NPs, but their toxicity could still be observed. Although the core/shell structures were slightly more toxic than the TiO_2 NPs, their degree of oxidative stress was less than that of the ZnO+TiO_2 NP mixtures. Furthermore, the cytotoxicity of the core/shell NPs decreased upon increasing the extent of coating. The decrease of ZnO toxicity arose presumably because (i) less of the nano-ZnO interacted with the cells, and (ii) the rate of zinc ion release from the ZnO cores decreased. In summary, we have developed a new approach for evaluating the toxicity of core/shell NPs, finding that TiO_2 shell coatings decrease the toxicity of ZnO NPs.

AUTHOR INFORMATION

Corresponding Author

*Phone: +886-3-5715131 ext. 35496. Fax: +886-3-5718649. E-mail: yjhuang@mx.nthu.edu.tw.

Funding Sources

This study was supported financially by a research grant from the National Science Council, Taiwan.

ACKNOWLEDGMENT

We thank Drs. Jyh-Fu Lee and Ling-Yun Jang, Beamline 17C and 16A spokespersons at the National Synchrotron Radiation Research Center, Taiwan, for conducting the XAS experiments. We thank Associate Professors Chien-Hou Wu and Chun-Yu Cheryl Chuang, Department of Biomedical Engineering and Environmental Sciences, National Tsing-Hua University, for help with the DLS and ELISA assays. Thanks also to the editor Dr. Chris A. Bradfield and five anonymous (unknown) reviewers for their comments.

ABBREVIATIONS

SiO_2, nanosilicon dioxide; CdSe, nanocadmium selenide; Au, gold NPs; Fe_2O_3, nanoiron(III) oxide; CdS, nanocadmium sulfide; CdTe, cadmium telluride; nano-ZnO, nanozinc oxide;

ZnO/TiO_2, TiO_2-coated ZnO NPs; TiO_2, nanotitanium dioxide; QDs, quantum dots; A549, human lung epithelial cells; W, watt; TEM, transmission electron microscopy; XRD, X-ray diffraction; XAS, X-ray absorption spectroscopy; XANES, X-ray absorption near edge structure; EXAFS, extended X-ray absorption fine structure; CN, coordination number; ICP-OES, inductively coupled plasma optical emission spectrometry; ICP-MS, inductively coupled plasma mass spectrometry; DLS, diffraction laser scattering; ROS, reactive oxygen species; LDH, lactate dehydrogenase; MTT, methyl tetrazolium cytotoxicity; DCFH-DA, 2′,7′-dichlorofluorescin diacetate; DCF, dichlorofluorescein; IL-8, interleukin-8.

REFERENCES

(1) Wang, L. N., and Muhammed, M. (1999) Synthesis of zinc oxide nanoparticles with controlled morphology. *J. Mater. Chem. 9*, 2871–2878.

(2) Meulenkamp, E. A. (1998) Synthesis and growth of ZnO nanoparticles. *J. Phys. Chem. B 102*, 5566–5572.

(3) Song, Z., Li, Q., and Gao, L. J. (1997) Preparation and properties of nano-TiO_2 powders. *J. Mater. Sci. Technol. 13*, 321–323.

(4) Zhuang, J., Liu, M., and Liu, H. B. (2009) MAA-modified and luminescence properties of ZnO quantum dots. *Sci. China Ser. B 52*, 2125–2133.

(5) Usui, H. (2009) The effect of surfactants on the morphology and optical properties of precipitated wurtzite ZnO. *Mater. Lett. 63*, 1489–1492.

(6) Li, F., Huang, X. T., Jiang, Y., Liu, L. Y., and Li, Z. (2009) Synthesis and characterization of ZnO/SiO_2 core/shell nanocomposites and hollow SiO_2 nanostructures. *Mater. Res. Bull. 44*, 437–441.

(7) Kim, S., Fisher, B., Eisler, H. J. Bawendi, M. Type-II quantum dots: CdTe/CdSe(core/shell) and CdSe/ZinTe(core/shell) heterostructures. *J. Am. Chem. Soc. 125*, 11466−11467.

(8) Tak, Y., Hong, S. J., Lee, J. S., and Yong, K. (2009) Fabrication of ZnO/CdS core/shell nanowire arrays for efficient solar energy conversion. *J. Mater. Chem. 19*, 5945–5951.

(9) Kim, C., Choi, M., and Jang, J. (2010) Nitrogen-doped SiO_2/TiO_2 core/shell nanoparticles as highly efficient visible light photocatalyst. *Catal. Commun. 11*, 378–382.

(10) Li, N. F., Lei, T., Ouyang, C., He, Y. H., and Liu, Y. (2009) An amperometric enzyme biosensor based on in situ electrosynthesized core/shell nanoparticles. *Synth. Met. 159*, 1608–1611.

(11) Chen, F., Bu, W. B., Chen, Y., Fan, Y. C., He, Q. J., Zhu, M., Liu, X. H., Zhou, L. P., Zhang, S. J., Peng, W. J., and Shi, J. L. (2009) A sub-50-nm monosized superparamagnetic Fe_3O_4@SiO_2 T-2-weighted MRI contrast agent: Highly reproducible synthesis of uniform single-loaded core/shell nanostructures. *Chem. Asian J. 4*, 1809–1816.

(12) Yang, P. P., Quan, Z. W., Hou, Z. Y., Li, C. X., Kang, X. J., Cheng, Z. Y., and Lin, J. (2009) A magnetic, luminescent and mesoporous core/shell structured composite material as drug carrier. *Biomaterials 30*, 4786–4795.

(13) Zhou, X. P., Kobayashi, Y., Romanyuk, V., Ochuchi, N., Takeda, M., Tsunekawa, S., and Kasuya, A. (2005) Preparation of silica encapsulated CdSe quantum dots in aqueous solution with the improved optical properties. *Appl. Surf. Sci. 242*, 281–286.

(14) Bao, F., Yao, J. L., and Gu, R. A. (2009) Synthesis of magnetic Fe_2O_3/Au core/shell nanoparticles for bioseparation and immunoassay based on surface-enhanced Raman spectroscopy. *Langmuir 25*, 10782–10787.

(15) He, Y., Lu, H. T., Sai, L. M., Lai, W. Y., Fan, Q. L., Wang, L. H., and Huang, W. (2006) Microwave-assisted growth and characterization of water-dispersed CdTe/CdS core/shell nanocrystals with high photoluminescence. *J. Phys. Chem. B 110*, 13370–13374.

(16) Yang, G. C. C., and Chan, S. W. (2009) Photocatalytic reduction of chromium(VI) in aqueous solution using dye-sensitized nanoscale ZnO under visible light irradiation. *J. Nanopart. Res. 11*, 221–230.

(17) Senthilkumar, K., Senthilkumar, O., Yamauchi, K., Sato, M., Morito, S., Ohba, T., Nakamura, M. Fujita, Y. Preparation of ZnO nanoparticles for bio-imaging applications. *Phys. Status Solidi B 246*, 885−888.

(18) Li, Y. Z., Xie, W., Hu, X. L., Shen, G. F., Zhou, X., Xiang, Y., Zhao, X. J., and Fang, P. F. (2010) Comparison of dye photodegradation and its coupling with light-to-electricity conversion over TiO_2 and ZnO. *Langmuir 26*, 591–597.

(19) Khodja, A. A., Sehili, T., Pilichowski, J. F., and Boule, P. (2001) Photocatalytic degradation of 2-phenylphenol on TiO_2 and ZnO in aqueous suspensions. *J. Photochem. Photobiol. A 141*, 231–239.

(20) Adams, L. K., Lyon, D. Y., and Alvarez, P. J. J. (2006) Comparative eco-toxicity of nanoscale TiO_2, SiO_2, and ZnO water suspensions. *Water Res. 40*, 3527–3532.

(21) Deng, X. Y., Luan, Q. X., Chen, W. T., Wang, Y. L., and Jiao, Z. (2009) Nanosized zinc oxide particles induce neural stem cell apoptosis. *Nanotechnology 20*, 115101.

(22) Sharma, V., Shukla, R. K., Saxena, N., Parmar, D., Das, M., and Dhawan, A. (2009) DNA damaging potential of zinc oxide nanoparticles in human epidermal cells. *Toxicol. Lett. 185*, 211–218.

(23) Gojova, A., Guo, B., Kota, R. S., Rutledge, J. C., Kennedy, I. M., and Barakat, A. I. (2007) Induction of inflammation in vascular endothelial cells by metal oxide nanoparticles: Effect of particle composition. *Environ. Health Perspect. 115*, 403–409.

(24) Liao, M. H., Hsu, C. H., and Chen, D. H. (2006) Preparation and properties of amorphous titania-coated zinc oxide nanoparticles. *J. Solid State Chem. 179*, 2020–2026.

(25) Wu, W., Cai, Y. W., Chen, J. F., Shen, S. L., Martin, A., and Wen, L. X. (2006) Preparation and properties of composite particles made by nano zinc oxide coated with titanium dioxide. *J. Mater. Sci. 41*, 5845–5850.

(26) Kim, S. K., Kim, W. D., Kim, K. M., Hwang, C. S., and Jeong, J. (2004) High dielectric constant TiO_2 thin films on a Ru electrode grown at 250 °C by atomic-layer deposition. *Appl. Phys. Lett. 85*, 4112–4114.

(27) Soto, K. F., Carrasco, A., Powell, T. G., Murr, L. E., and Garza, K. M. (2006) Biological effects of nanoparticulate materials. *Mater. Sci. Eng. C 26*, 1421–1427.

(28) Cho, S. J., Maysinger, D., Jain, M., Roder, B., Hackbarth, S., and Winnik, F. M. (2007) Long-term exposure to CdTe quantum dots causes functional impairments in live cells. *Langmuir 23*, 1974–1980.

(29) Su, Y. Y., He, Y., Lu, H. T., Sai, L. M., Li, Q. N., Li, W. X., Wang, L. H., Shen, P. P., Huang, Q., and Fan, C. H. (2009) The cytotoxicity of cadmium based, aqueous phase−synthesized, quantum dots and its modulation by surface coating. *Biomaterials 30*, 19–25.

(30) Brunner, T. J., Wick, P., Manser, P., Spohn, P., Grass, R. N., Limbach, L. K., Bruinink, A., and Stark, W. J. (2006) In vitro cytotoxicity of oxide nanoparticles: Comparison to asbestos, silica, and effects of particle solubility. *Environ. Sci. Technol. 44*, 4373–4381.

(31) Souza, D. M., Andrade, A. L., Fabris, J. D., Valerio, P., Goes, A. M., Leite, M. F., and Domingues, R. Z. (2008) Synthesis and in vitro evaluation of toxicity of silica-coated magnetite nanoparticles. *J. Non-Cryst. Solids 354*, 4894–4897.

(32) Zhou, Y. P., Jia, X. E., Tan, L., Xie, Q. J., Lei, L. H., and Yao, S. Z. (2010) Magnetically enhanced cytotoxicity of paramagnetic selenium-ferroferric oxide nanocomposites on human osteoblast-like MG-63 cells. *Biosens. Bioelectron. 25*, 1116–1121.

(33) Du, H. C., Yuan, F. L., Huang, S. L., Li, J. L., and Zhu, Y. F. (2004) A new reaction to ZnO nanoparticles. *Chem. Lett. 33*, 770–771.

(34) Klug, H., and Alexander, L. (1954) *X-ray Diffraction Methods for Polycrystalline and Amorphous Materials*, John Wiley and Sons, New York.

(35) Kroll, A., Pillukat, M. H., Hahn, D., and Schekenburger, J. (2009) Current in vitro methods in nanoparticle risk assessment: Limitations and challenges. *Eur. J. Pharm. Biopharm. 72*, 370–377.

(36) Powers, K., Brown, S., Krishna, V., Wasdo, S., Moudgil, B., and Roberts, S. (2006) Research strategies for safety evaluation of

nanomaterials. Part VI. Characterization of nanoscale particles for toxicological evaluation. *Toxicol. Sci. 90*, 296–303.

(37) Yang, R. D., Tripathy, S., Li, Y. T., and Sue, H. J. (2005) Photoluminescence and micro-Raman scattering in ZnO nanoparticles: The influence of acetate adsorption. *Chem. Phys. Lett. 411*, 150–154.

(38) Zhang, H. Z., Luo, X. H., Xu, J., Xiang, B., and Yu, D. P. (2004) Synthesis of TiO_2/SiO_2 core/shell nanocable arrays. *J. Phys. Chem. B. 108*, 14866–14869.

(39) Zhang, H. Z., Chen, B., Banfield, J. F., and Waychunas, G. A. (2008) Atomic structure of nanometer-sized amorphous TiO_2. *Phys. Rev. B 78*, 214106.

(40) Farges, F., Brown, G. E., and Rehr, J. J. (1997) Ti K-edge XANES studies of Ti coordination and disorder in oxide compounds: Comparison between theory and experiment. *Phys. Rev. B 56*, 1809–1819.

(41) Chen, C. C., Chen, R. S., Tsai, T. Y., Huang, Y. S., Tsai, D. S., and Tiong, K. K. (2004) The growth and characterization of well aligned RuO_2 nanorods on sapphire substrates. *J. Phys.: Condens. Matter 16*, 8475–8484.

(42) Wilmer, H., Kurtz, M., Klementiev, K. V., Tkachenko, O. P., Grunert, W., Hinrichsen, O., Birkner, A., Rabe, S., Merz, K., Driess, M., Woll, C., and Muhler, M. (2003) Methanol synthesis over ZnO: A structure-sensitive reaction? *Phys. Chem. Chem. Phys. 5*, 4736–4742.

(43) Lim, S. H., Phonthammachai, N., Liu, T., and White, T. J. (2008) X-ray absorption spectroscopy studies of phase transformations and amorphicity in nanotitania powder and silica-titania core/shell photocatalysts. *J. Appl. Crystallogr. 41*, 1009–1018.

(44) Jeng, H. A., and Swanson, J. (2006) Toxicity of metal oxide nanoparticles in mammalian cells. *J. Environ. Sci. Health, Part A 41*, 2699–2711.

(45) Lin, W. S., Xu, Y., Huang, C. C., Ma, Y. F., Shannon, K. B., Chen, D. R., and Huang, Y. W. (2009) Toxicity of nano- and micro-sized ZnO particles in human lung epithelial cells. *J. Nanopart. Res. 11*, 25–39.

(46) Braydich-Stolle, L. K., Schaeublin, N. M., Murdock, R. C., Jiang, J., Biswas, P., Schlager, J. J., and Hussain, S. M. (2009) Crystal structure mediates mode of cell death in TiO_2 nanotoxicity. *J. Nanopart. Res. 11*, 1361–1374.

(47) Jiang, J., Oberdorster, G., Elder, A., Gelein, R., Mercer, P., and Biswas, P. (2008) Does nanoparticle activity depend upon size and crystal phase? *Nanotoxicology 2*, 33–42.

(48) Nel, A., Xia, T., Madler, L., and Li, N. (2006) Toxic potential of materials at the nanolevel. *Science 311*, 622–627.

(49) Lenz, A. G., Karg, E., Lentner, B., Dittrich, V., Brandenberger, C., Rothen-Rutishauser, B., Schulz, H., Ferron, G. A., and Schmid, O. (2009) A dose-controlled system for air−liquid interface cell exposure and application to zinc oxide nanoparticles. *Part. Fibre Toxicol. 6*, 32.

(50) Singh, S., Shi, T. M., Duffin, R., Albrecht, C., van Berlo, D., Hoehr, D., Fubini, B., Martra, G., Fenoglio, I., Borm, P. J. A., and Schins, R. P. F. (2007) Endocytosis, oxidative stress and IL-8 expression in human lung epithelial cells upon treatment with fine and ultrafine TiO_2: Role of the specific surface area and of surface methylation of the particles. *Toxicol. Appl. Pharmacol. 222*, 141–151.

(51) Moos, P. J., Chung, K., Woessner, D., Honeggar, M., Cutler, N. S., and Veranth, J. M. (2010) ZnO particulate matter requires cell contact for toxicity in human colon cancer cells. *Chem. Res. Toxicol. 23*, 733–739.

(52) Hanley, C., Thurber, A., Hanna, C., Punnoose, A., Zhang, J. H., and Wingett, D. G. (2009) The influences of cell type and ZnO nanoparticle size on immune cell cytotoxicity and cytokine induction. *Nanoscale Res. Lett. 4*, 1409–1420.

(53) Jin, C. Y., Zhu, B. S., Wang, X. F., and Lu, Q. H. (2008) Cytotoxicity of titanium dioxide nanoparticles in mouse fibroblast cells. *Chem. Res. Toxicol. 21*, 1871–1877.

(54) Yang, H., Liu, C., Yang, D. F., Zhang, H. S., and Xi, Z. G. (2009) Comparative study of cytotoxicity, oxidative stress and genotoxicity induced by four typical nanomaterials: The role of particle size, shape and composition. *J. Appl. Toxicol. 29*, 69–78.

(55) Xia, T., Kovochich, M., Liong, M., Madler, L., Gilbert, B., Shi, H., Yeh, J. I., Zink, J. I., and Nel, A. E. (2008) Comparison of the mechanism of toxicity of zinc oxide and cerium oxide nanoparticles based on dissolution and oxidative stress properties. *ACS Nano 2*, 2121–2134.

(56) George, S., Pokhrel, S., Xia, T., Gilbert, B., Ji, Z. X., Schowalter, M., Rosenauer, A., Damoiseaux, R., Bradley, K. A., Madler, L., and Nel, A. E. (2010) Use of a rapid cytotoxicity screening approach to engineer a safer zinc oxide nanoparticle through iron doping. *ACS Nano 4*, 15–29.